# THERMOGRAPHIC DEFECTOSCOPY OF MATERIALS IN NUCLEAR POWER ENGINEERING BASED ON THE ANALYSIS OF THE NORMALIZED COEFFICIENT OF THE DYNAMICS OF THERMOPRODUCTION OF DEFECTS AT INDUCTION ACTIVATION

***N.I. Bazaleev, V.V. Lytvynenko***
***Institute of Electrophysics and Radiation Technologies NAS of Ukraine,***
***Kharkov, Ukraine***
***E-mail: ntcefo@yahoo.com***

The features of induction thermography for flaw detection of ferromagnetic materials used in nuclear power engineering are considered. A technique for thermographic defectoscopy of ferromagnetic materials based on dynamic contrast analysis of thermal images and the normalized coefficient of thermal manifestation of defects at the electromagnetic activation of samples is proposed. The materials of experimental studies confirming the efficiency of using low-frequency (50 Hz) inductors in thermographic defectoscopy, the possibility of identifying thermal manifestations of defects against a background of false thermoanomalies by monitoring the change in the thermodynamic temperature in the region of defects during induction activation are presented.

PACS: 65.90.+I

## INTRODUCTION

Intensive development of thermal imaging technology and methods of thermographic defectoscopy makes it possible to increase the efficiency of control of structural materials and assess the condition of aging technological equipment and facilities of a nuclear power complex. Thermal imaging thermography, the accelerated development of which has recently been restrained by the imperfection of existing techniques and hardware, is one of the promising directions and methods of nondestructive testing suitable for use in nuclear power engineering. The Institute of Electrophysics and Radiation Technologies (IERT) of the National Academy of Sciences of Ukraine, within the framework of the State Program of Fundamental and Applied Research on the Use of Nuclear Materials and Nuclear and Radiation Technologies in the Sphere of Development of the Regions of the Economy, is developing new methods of thermal imaging diagnostics, thermal imaging operational control systems for operational characteristics and diagnostics on their basis of the technical condition of equipment, facilities and communications of nuclear power plants. Our studies show that thermal imaging provides the ability to solve a wide range of problems when inspecting technological equipment and structures. When solving the issue of extending the service life and carrying out technical inspection of pipelines and technical water supply system of the responsible consumers of group "A" of power units 1-6 of Zaporizhzhya NPP, IERT NAS of Ukraine thermal imaging studies were carried out, which allowed obtaining various information on the condition of underground pipelines, the expediency of thermal imaging control of equipment and structures, conjugated with pipelines, Fig. 1.

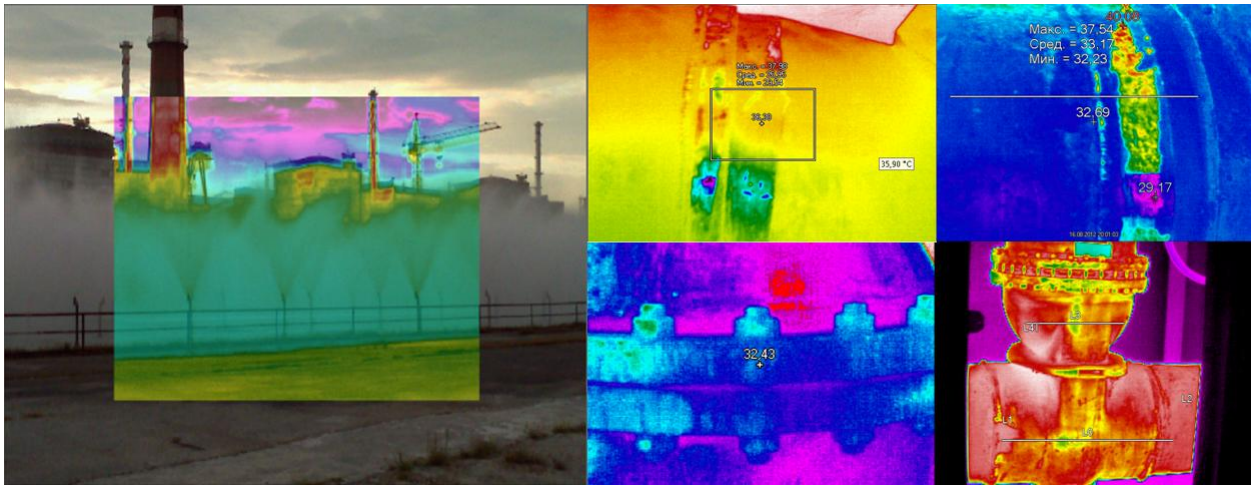


*Fig. 1. Zaporizhzhya NPP. Thermal imaging monitoring of the condition of pipelines and the technical water supply system of the responsible consumers of group "A" (fragments of thermal manifestation in the field of infrared radiation of structural inhomogeneities/defects on pipelines and fittings of the objects surveyed are given)*

At the same time, the improvement and optimization of this promising methodology and its adaptation to the tasks of establishing and prolonging the life of nuclear power plant equipment requires the solution of a number of scientific and technical problems, in particular, the development of new approaches to

solving the problems of the physics of dissipative systems and thermal processes that occur in materials and structural elements of survey objects. Obvious is the need to improve the methods of thermographic analysis, which allow for the controls dynamics of the development of the temperature field in the vicinity of defects (cracks) for revealings structural changes in structural materials. The growth of scientific interest in new approaches to thermographic diagnostics [1–3] not only indicates a desire to increase the reliability of the results of thermographic flaw detection, but also a palpable lack of information about the features of the thermal manifestation of defects in active thermography, the search for new informative characteristics of defects in the parameters of the physical fields that determine degree of their danger.

Of the existing inspection methods of thermographic control, active methods are the most developed, which differ in the way the heat energy is introduced into the sample and its response, which changes the temperature both in the defect region and on the sample surface [4–6]. In active thermography, an external energy action sufficient to transfer the sample to the thermodynamic state, which provides the necessary level of the thermal contrast of thermoimages of structural inhomogeneities, is used to activate the thermal manifestation of defective structures/defects. External energy impact can be thermal activation, providing direct heating / cooling of the sample, and also acoustic or electromagnetic (inductive) activation, which based on the use of thermophysical effects of the transformation of wave energy into heat when interacting with the environment of the object of control. With the electromagnetic activation of ferromagnetic materials, the energy losses on eddy currents and hysteresis in the form of heat are differentiated on inhomogeneities whose thermophysical properties differ from the characteristics of the article material and are reflecting on the thermoimage of the monitoring object. Low-frequency induction activation has a number of advantages over conventional active thermography due to the possibility of rapid direct heating of the sample and a large depth of penetration of electromagnetic radiation into the ferromagnet, which provides an effective differentiation of the surface temperature between the defect and the defect-free zone, depending on the magnetic and thermophysical properties of the defect, its dimensions and depth of occurrence. This allows us to detect thermo-manifestations of macro- and microstructural inhomogeneities, areas of plastic deformation, discontinuity defects, cracks, etc., by the dynamics of the change in the parameters of thermoimages [7, 8]. It should be taken into account that the internal and external factors that form false thermoanomalies (including due to variations in the radiation emissivity of the surface of the monitoring object) have a significant influence on the formation of thermoimages of the monitoring object, which in amplitude can significantly exceed the thermal manifestations of defective structures.

## 1. PRINCIPLE OF NORMALIZATION OF THERMAL MANIFESTATION OF DEFECTS IN ACTIVE THERMOGRAPHY

One of the common methods for identifying thermal manifestations of structural inhomogeneities in metals is the method of temperature contrast, based on fixing temperature differences on the surface of the object under study and a more detailed examination of zones with an elevated/lower temperature. Although the raised/lowered temperature is not always a sign of the presence of a defect, the temperature contrast method can be successfully used for flaw detection of ferromagnetic materials.

The methodology of low-frequency (50 Hz) induction thermography is described in [9] for the detection of defects on flat surfaces of ferromagnetic materials on the basis of an analysis of the thermal processes of formation of a temperature field in the defect region [10] and a dipole model [11, 12] that takes into account tangential ($H_x$) and the normal ($H_y$) components of the leakage magnetic field at the point ($x$, $y$). The features of the thermal manifestation of artificially created defects (rectangular slits of different depths) are studied at activation time from 20 to 100 sec. It is shown that such defects are easily identified by their thermal manifestation, while the temperature difference between the defect and the region without a defect or regions with smaller defects is 0.15…2 °C. The authors of [13] proposed a method of thermal contrast analysis based on the use of normalized thermal contrast:

$$C_i(t) = \frac{T_{def}(t) - T_{def}(t_0)}{T_{sdef}(t) - T_{sdef}(t_0)}, \quad (1)$$

where $C_i(t)$ – is the normalized thermal contrast at point (**i**) at time (**t**); $T_{def}(t), T_{sdef}(t)$ – surface temperature in the defective and defect-free point, respectively.

Considering the high efficiency of use $C_i(t)$ in studying the dynamics of temperature fields in the vicinity of defects, we proposed a technique for identifying thermal manifestations of defects against a background of noise in induction thermography by modifying the coefficient $C_i(t)$ into the normalized coefficient of the thermal manifestation of the defect $K_{TD}$. $K_{TD}$ allows to take into account the change in the radiation and thermodynamic (true) temperature at any point on the thermoimage of the sample surface:

$$K_{TD}\big|_{t_2,t_3,t_{4...}} = \frac{T_{R/D}(t) - T_{R/D}(t_1)}{T_{R/DF}(t) - T_{R/DF}(t_1)} = \\ = \frac{\varepsilon_1}{\varepsilon_2} \times \frac{T^4_{T/D}(t) - T^4_{T/D}(t_1)}{T^4_{T/DF}(t) - T^4_{T/DF}(t_1)} = \frac{\varepsilon_1}{\varepsilon_2} \times K_{TA}\big|_{t_2,t_3,t_{4...}}, \quad (2)$$

where $T_{R/D}(t_1), T_{R/D}(t)$ and $T_{R/DF}(t_1), T_{R/DF}(t)$ is the radiation temperature at points located in the zones of the alleged defect and in the defect-free zone at the instants of time $t_1$ – the activation beginning,

$t = t_2, t_3, t_4 \ldots$ – in the process of sample activation (here $T_R \sim R_e = \varepsilon\sigma T_T^4$; $T_R$, $T_T$ – is the radiation and thermodynamic (true) temperature of the sample, respectively; $R_e$ – the energy luminosity recorded by the thermal imager; $\varepsilon$ – the emissivity of the external surface of the sample); $\varepsilon_1$ and $\varepsilon_2$ – is the radiation coef-ficients at points located in the defect zone and the defect-free zone, respectively; $\sigma$ – is the Stefan-Boltzmann constant; $K_{TA}$ – is the amplitude of the thermal anomaly amplitude.

As we can see, the radiation temperature $T_R$ recorded by the thermal imager and thermal anomalies $\pm\Delta T_R$ on the thermal image depend both on the thermodynamic temperature $T_T$, and the emissivity $\varepsilon$ of the external surface of the monitoring object. If the thermodynamic temperatures in the zones (points) of the supposed defect and the defect-free zone are equal, ie, $T_{T/D} = T_{T/DF}$ (the sample is in the isothermal state), the normalized coefficient of thermal manifestation $K_{TD}$ is a constant during the whole activation cycle of the sample, while:

$$K_{TD}\,|_{t_2,t_3,t_{4\ldots}} = \frac{\varepsilon_1}{\varepsilon_2} = const,$$

$$K_{TA}\,|_{t_2,t_3,t_{4\ldots}} = 1. \qquad (3)$$

In this case, the cause of thermal anomaly in the zone of the alleged defect is the anomalous value of the radiation coefficient $\varepsilon_1$.

If the thermoanomaly is caused by the change in the thermodynamic temperature $T_T$ in the zone of the expected defect, which differs from the true temperature $T_{T/DF}$ of the defect-free zone by $\pm\Delta T_T$. Wherein: $T_{T/D} = T_{T/DF} \pm \Delta T_T$, $T_{RD} \sim \varepsilon_1\sigma(T_{T/DF} \pm \Delta T_T)^4$, the coefficient $K_{TA}$ of the thermal anomaly is determined as:

$$K_{TA}\,|_{t_2,t_3,t_{4\ldots}} = \frac{(T_{T/DF}(t) \pm \Delta T_T(t))^4 - T_{T/DF}^4(t_1)}{T_{T/DF}^4(t) - T_{T/DF}^4(t_1)} \neq 1. \qquad (4)$$

In the process of sample activation under the thermodynamic character of the manifestation of the defect, the coefficient $K_{TD}$, determined at the instants of time $t_2, t_3, t_4 \ldots$, has different values (increases or decreases depending on the sign $\pm$ of thermal anomaly $\Delta T_{TT}$). The algorithm for processing thermal information that provides identification of thermal manifestations of defects against a background of false thermal anomalies is shown in Fig. 2 At the same time, the initial information is a map (thermal image) obtained by means of an IR radiometric device (thermal image) of the distribution of radiation temperature on the surface of the object of investigation, which is in the thermodynamic state under the action of the activation energy for a time $t = t_2, t_3, t_4 \ldots$

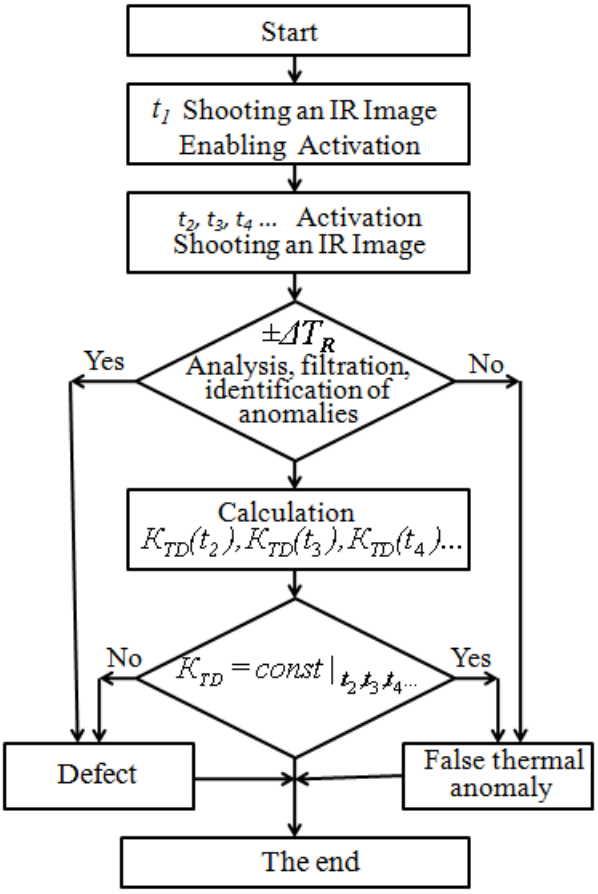


*Fig. 2. Algorithm for identifying thermal manifestations of defects against a background of false thermoanomalies*

## 2. RESULTS OF EXPERIMENTAL STUDIE

Below are examples of identification of thermal manifestations of defects on the background of false thermal anomalies on the basis of an analysis of the normalized coefficient of thermal manifestation of defects on IR images of ferromagnetic samples with artificially created defects of different depth and orientation with respect to the magnetic flux of the low-frequency (50 Hz) activator [7, 8].

Fig. 3 shows a photo image of a specimen of a plate made of ferromagnetic material (rolling steel Ст.30, dimensions 130x60x5 mm, artificially created defects: transverse "through crack" **A**$_{\mathbf{C}}$ 17x5x1 mm against a background of "blind crack" **A** 45x4x1 mm variable 1…3.5 mm depth, transverse "blind crack" **B** 45x4x1 mm variable 1…3.5 mm depth, the area of corrosion-erosion damage to the surface of the sample, depth of erosion 0.1…0.2 mm). Activation of a flat sample was carried out for 50 s in the working area of the electromagnetic activator EMA (induction coil with a U-shaped magnetic core. The working zone is located between the poles of the magnetic circuit). Figure shows

the thermoimages (Fig. 4) and thermo-grams (Fig. 5) along the **LO** section of the sample at the beginning ($t_1$), at 13 ($t_4$) and 26 ($t_8$) seconds of activation. To identify the features of the change in the coefficient $K_{TD}$ on the thermal anomalies caused by thermal manifestations of defects and false anomalies, control points **1–7** were marked on the thermoimages (see Fig. 3), indicating the location of their location on the sample (see the photo image in Fig. 3,b). Point **1** is located directly on the through crack of the $\mathbf{A_C}$; point **2** – defect-free, reference point; point **3** – is located on the invisible side of the crack **A**; point **4** – is located on a false thermal anomaly due to the Narcissus effect (reflected radiation of the optical system of the thermal imager); point **5** – located on the invisible side of the crack **B**; points **6, 7** – located in the area of corrosion-erosion damage to the surface of the sample.

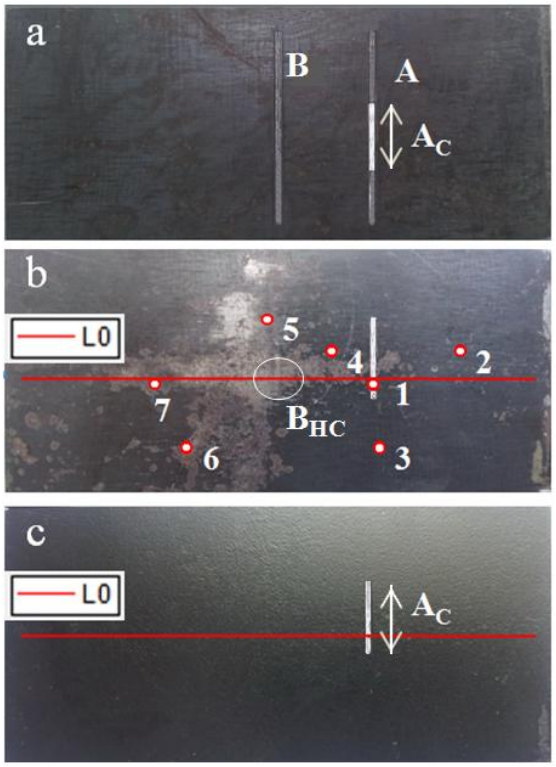


*Fig. 3. Photographs of ferromagnetic samples of a plate with artificially created defects: a – an invisible side indicating the shape of the defect section; b – a visible side with points and a thermographic inspection profile; c – a visible side with a painted coating*

Thermal images of the plate (see Fig. 3) clearly show the "through crack" thermoanomals of the $\mathbf{A_C}$, the area of corrosion-erosion damage (points **7, 6**) and the region of variation of the emissivity of the plate surface. The relative change in the amplitude of the anomalies on the defects at 13 and 26 s of activation of the sample at points **1, 3, 5** relative to defect-free point **2** is: point **1**(-2.5 °C and -6.4 °C), point **3** (1.6 °C and 1.6 °C), point 5 (-1.0 °C and -2.6 °C), points **6, 7** (-1.5 °C and 2.4 °C), (0.15 °C and -0.65 °C) respectively, at the point **4** of the false thermoanomaly (-1.4 °C and -2.6 °C).

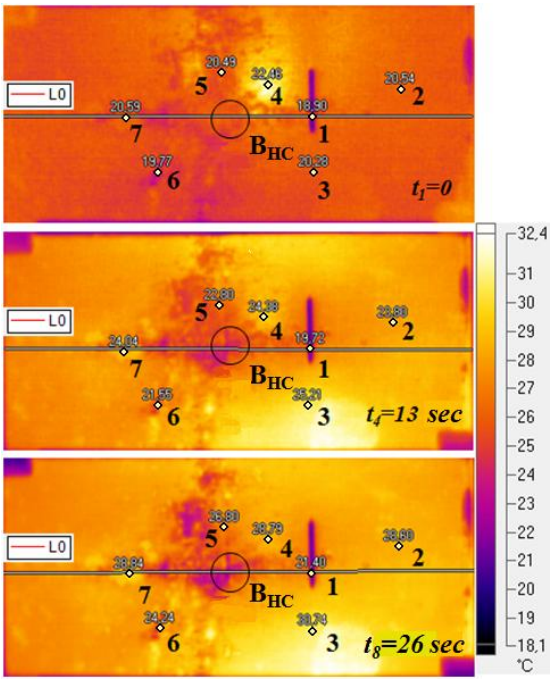


*Fig. 4. Thermal imaging of the plate in the working area of the electromagnetic activator: **1** – thermoimage of the plate at the beginning ($t_1$), at **13** ($t_4$) and **26** ($t_8$) s of sample activation*

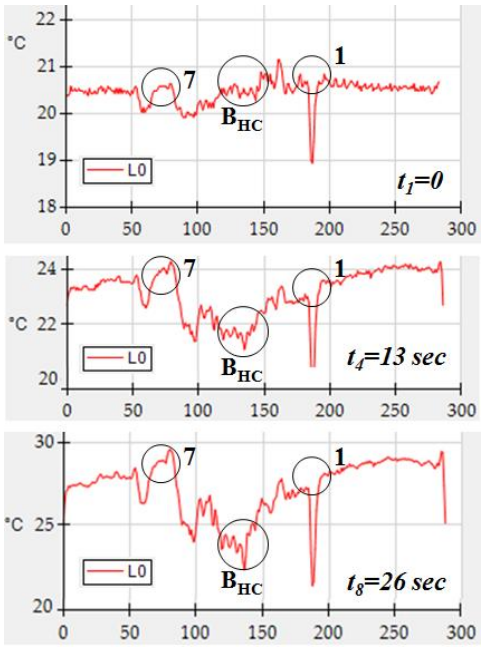


*Fig. 5. Thermograms along the section line **LO** of the sample at the beginning ($t_1$), at **13** ($t_4$) and **26** ($t_8$) seconds of sample activation*

The greatest amplitude of thermal anomaly relative to a defect-free point **2** is observed at the point **4** ($\Delta T_R$ = 2 °C at $t_1 = 0$) on a false thermoanomaly (Narcissa effect) located in the area of corrosion-erosion damage of the sample surface. At the through crack (point **1**) $\Delta T_R$ = -1.6 °C, on the invisible side of the crack **A** (point **3**) – $\Delta T_R$ = -0.2 °C, on the invisible side of the crack **B** (point **5**) – $\Delta T_R$ = 0.0 °C. At the beginning of the activation, the contrast increases in the defect region, and then because of the high thermal

conductivity of the metal and the duration of the activation process of the sample (in our case more than 50 s), the thermal contrast decreases due to the temperature increase of the sample as a whole.

On the thermograms (see Fig. 5) along the section line of the sample **L0**, thermal anomalies in the region of the through crack of the $\mathbf{A_C}$ (point **1**), the hidden crack **B** (the $\mathbf{B_{HC}}$ section), and the surface defect in the region of the point **7** are fairly clearly manifested. At the same time, the amplitude of the thermal manifestation of the defects increases with increasing activation time.

When calculating the coefficients of thermal manifestation of defects $K_{TD}$ (Fig. 6), averaging methods and filtering of high-frequency components of fluctuations in the radiation temperature at the control points were used methods of averaging and filtering the high-frequency components of fluctuations in the radiation temperature at the control points were used.

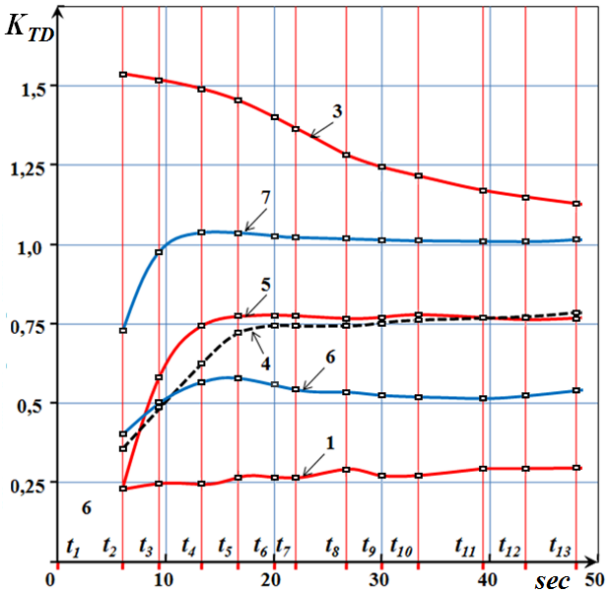


*Fig. 6. Change in the coefficient of thermal manifestation of defects $K_{TD}$ in the selected points of the control of thermal anomalies in the process of electromagnetic activation of the plate*

As can be seen, practically for all control points (except point **1**), the coefficient $K_{TD}$ has the thermodynamic character of the appearance of thermoanomalies (i. e., $K_{TA} \neq 1$ and the coefficient $K_{TD}$, determined at time instants $t_2, t_3, t_4 \ldots$, has different values). The greatest change in the coefficient $K_{TD}$ occurs in the initial stage of sample activation (10…15 s) due to a local change in the thermodynamic temperature in the defect region (Joule heat effect). Then, the temperature of the sample is equalized by thermal diffusion. The through crack (point **1**) in this case behaves like an absolutely black body whose temperature corresponds to the background temperature (point **2**) of the sample and $K_{TA} = 1$. The change in the coefficient $K_{TD}$ at point **4** is due to the thermodynamic character of the thermal manifestation of corrosion-erosion damage, which at the initial stage of sample activation was screened by a false (Narcissa effect) thermoanomaly.

Investigation of the features of the thermal manifestation of artificially created defects on cylindrical ferromagnetic samples was carried out by placing an experimental sample inside two induction coils of the electromagnetic activator EMA [7, 8], between which there was a working zone of thermo-graphic control. Sample activation time 170 s. The experimental sample (Fig. 7) is made of a piece of pipe (steel Ст.30, sample length 350 mm, diameter 60 mm, wall thickness 3 mm). Artificially created defects **D1, D2,** and **D3** are filled with a mineral mixture: **D1** – longitudinal "through crack" (50x3x1 mm), control point 2; **D2** – transverse "through crack" (35x3x1 mm), control point 4; **D3** – rivet type defect with a diameter of 6 mm, control point **1**.

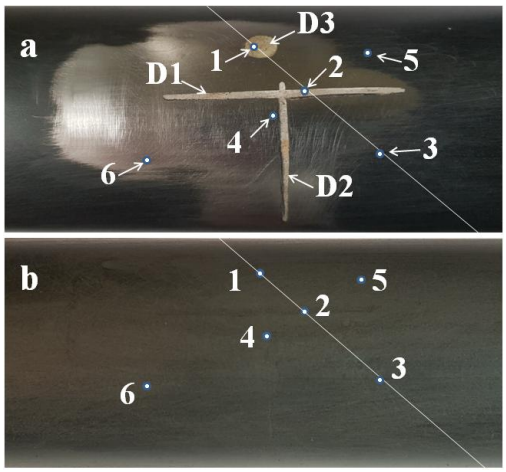


*Fig. 7. Photographs of ferromagnetic samples section of pipe with artificially created defects: a – layout of defects **D1 – D3** with points and lines of section **LO** of thermographic inspection; b – visible side of pipe section with painted coating*

Figure shows the thermal images (Fig. 8) and the thermograms (Fig. 9) the section line of the **LO** fragment of the pipe in the working area of the activator at the beginning ($\mathbf{t_1}$), at 41 ($\mathbf{t_3}$) and 107 ($\mathbf{t_6}$) seconds of activation. The maximum amplitude of the thermal anomaly ($\Delta T_R$ = 0.9 °C) is observed on the "false defect" in the thermoimage of the tube fragment (see Fig. 8), taken at the beginning of the sample activation process ($\mathbf{t_1}$ = 0), point **3**; on the "false defect" (point **6**) $\Delta T_R$ = 0.2 °C. On the defects **D1, D2,** and **D3**, the anomaly amplitude $\Delta T_R$ is 0.5 °C (point **2**), 0.4 °C (point **4**), and 0.3 °C (point **1**), respectively. At the beginning of the sample activation process, an increase in the contrast of the thermal image is observed, while the relative change in the amplitude of the anomalies on defects at 41 and 107 s of activation is: point **1** (-0.25 °C and 0.1 °C), point **2** (0.3 °C and 0.8 °C) , point **4** (-0.25 °C and 0.1 °C); on false thermal anomalies: point **3** (0.2 °C and 0.2 °C), point **6** (0.3 °C and 0.4 °C). The maximum thermal manifestation is observed at the defect **D1** "longitudinal crack" (point **2**) and also on the "false defect"", the control point **3**.

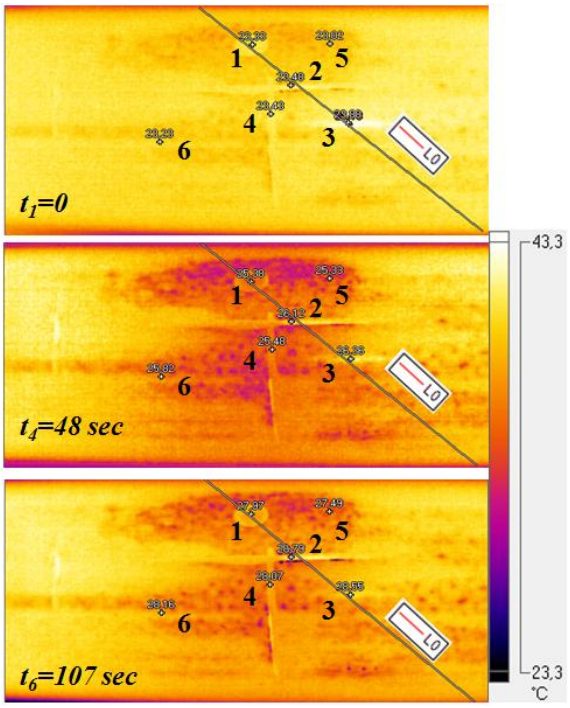


*Fig. 8. Thermal imaging of the pipe fragment in the working area of the electromagnetic activator. Thermoimage at the beginning (**$t_1$**), at 48 (**$t_4$**) and 107 (**$t_6$**) s of sample activation; 2 – thermograms along the section line **LO** of the sample at the beginning (**$t_1$**) and at 41 (**$t_3$**) and 107 (**$t_6$**) s of sample activation*

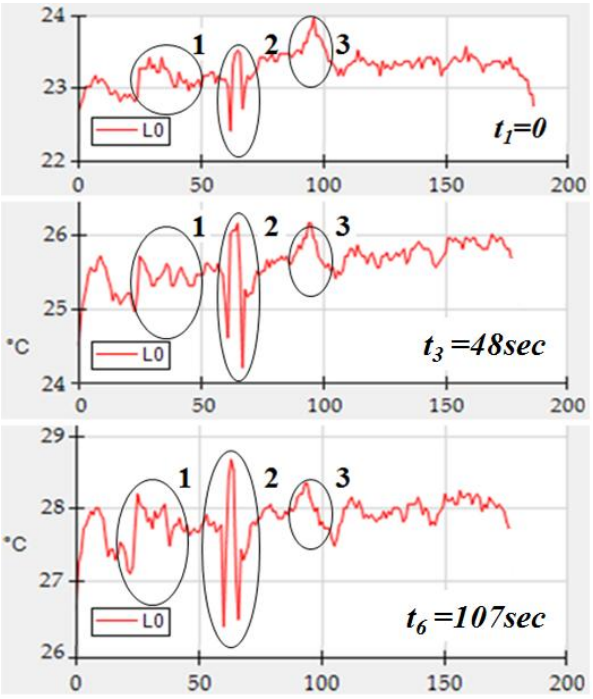


*Fig. 9. Thermograms along the section line **LO** of the sample at the beginning (**$t_1$**), at 41 (**$t_4$**) and 107 (**$t_6$**) s of sample activation*

The graph of the change in the thermal manifestation coefficient of the defects $K_{TD}$ (see Fig. 9) confirms the local character of the change in the thermodynamic temperature at the control points **1**, **2**, and **4** of the defects considered (the value $K_{TD}$ varies with time in the process of sample activati-on and $K_{TA} \neq 1$). On "false defects" (points **3** and **6**) the coefficient changes $K_{TD}$ are insignificant (i. e. $K_{TA} = 1$). The greatest change in the coefficient $K_{TD}$ occurs in the initial stage (20…70 s) of activation of the sample. With a further increase in the activation time, because of the high thermal conductivity of the metal, the temperature of the entire sample increases, which leads to a decrease in the thermal contrast of the thermal manifestations of the defects. It should be noted that with the prolonged action of the activator windings due to their heating, an additional thermal source of activation of the sample in the working zone arises due to the heating of those parts that are inside the EMA coils. Simultaneous action of the electromagnetic and thermal activators enhances the thermal manifestation of defects (control points **1**, **2, 4**) due to the action of the synergistic effect (Fig. 10).

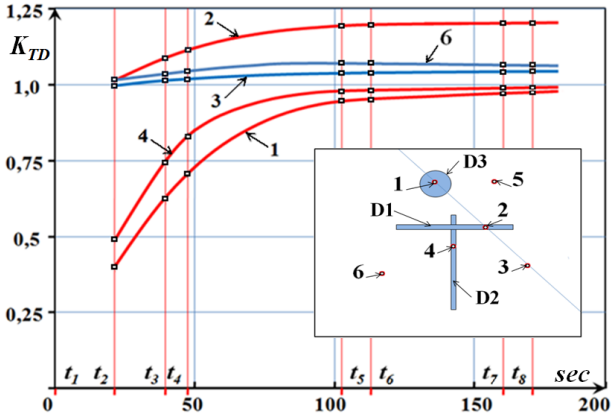


*Fig. 10. Change in the coefficient of thermal manifestation of defects $K_{TD}$ in the selected points of the control of thermal anomalies in the process of electromagnetic activation of the pipe segment*

## CONCLUSIONS

From the wide arsenal of active methods of thermographic defectoscopy used in atomic engineering, special attention is paid to induction thermography, based on the activation of ferromagnetic materials by low-frequency (50 Hz) electromagnetic fields. The experience of using low-frequency electromagnetic activators confirms the possibility of using them to visualize the picture of the spatial distribution of defective structures in materials by their thermal manifestation in the IR-radiation field.

Effective differentiation and identification of thermal anomalies on the thermal manifestation of defects and false thermoanomalies is ensured by dynamic thermography, based on an analysis of the dynamics of thermal processes in the formation of a temperature field in the region of defects during inductive activation. The proposed method of dynamic contrast analysis based on the use of the normalized coefficient of the thermal manifestation of a defect, provides possibility into account the dynamics of the change in the radiation and thermodynamic temperature at any point on the thermal image of the sample,

identify thermal manifestations of defects against a background of false thermoanomalies.

As shown by experimental studies, for false thermoanomalies caused by a change in the emissivity, the normalized thermal manifestation of the defect remains constant throughout the entire activation cycle of the sample. Thermal manifestations of defects are characterized by a change in the thermodynamic temperature in the region of the defect due to the Joule heat of the induced eddy currents. In this case, the coefficient $K_{TD}$ has different values (increases or decreases depending on the sign of the thermoanomaly) throug-hout the time of activation of the sample. The data of experimental studies confirm the possibility of using low-frequency electromagnetic activators in thermo-graphic defectoscopy of ferromagnetic materials of considerable thickness (with activation time of 10…30 s) and can be successfully used in solving practical problems.

## REFERENCES


1. J. Vrana, M. Goldammer, J. Baumann, M. Rothe nf-usser, and W. Arnold. Mechanisms and models for crack detection with induction thermograph // *CP975, Revierof Quantitative Nonde-structive Evalution*. 2007, v. 27, p. 475-482.

2. P. Jäckel, U. Netzelmann Jäckel. The influence of external magnetic fields on crack contrast in magnetic steel detected by induction thermography // *11th International Conference on Quantitative InfraRed Thermography*, 11–14 June 2012, Naples Italy.

3. Stefan Koch. Inline inspection of hot-rolled steel products by heat flux thermography *// FOP Spring Conference*, Gothenburg, April 28th, 2015. Stefan Koch. Non-destructive testing of bars by inductive heat-fl ux thermography // *Millennium steel India.* 2014, p. 140-142.

4. N.I. Bazaleev, V.V. Bryuhovetskiy, V.F. Klepikov, V.V. Lytvynenko. Thermovision acoustic thermography constraction materials defectoscopy // *Problems of Atomic Scince and Technology*. 2011, N 2 (97), p.178-185.

5. M. Noethen, Y. Jia, N. Meyendorf. Simulation of the surface crack detection using inductive heated thermography // *Nondestruct. Test. Eval.* 2012, v. 27, p. 139-149.

6. P. Jackel, U. Netzelmann. The influence of external magnetic fields on crack contrast in magnetic steel detected by induction thermography // *Quant. Infrared Thermography J*. 2013, v. 10, p. 237-247.

7. М.І. Базалєєв, В.В. Брюховецький, В.Ф. Клепіков, В.В. Литвиненко. Термографічний контроль структурних порушень в феромагнітних матеріалах при активації електромагнітним полем // *Компрессорное и энергетическое машиностроение.* 2014, №3(37), с. 13-17.

8. М.І. Базалєєв, В.В. Брюховецький, В.Ф. Клепіков, В.В. Литвиненко. Застосування електромагнітної активації при термографічному контролі дефектів та структурних неоднорідностей в феромагнітних матеріалах // *Техническая драгностика и неразрушающий контроль*. 2016, №2, с. 50-60.

9. B.B. Lahiri, S. Bagavathiappan, C. Soumya, V. Mahendran, V.P.M. Pillai, John Philip,T. Jayakumar. Infrared thermography based defect detection in ferromagnetic specimens using a low frequency alternating magnetic field // *Infrared Physics & Technology*. 2014, v. 64, p. 125-133.

10. D. Vagner, B.I. Lembrikov, P. Wyder. *Electrod y-namics of Magnetoactive Media.* First ed., Sprin-ger-Verlag, Germany, 2004.

11. J. Philip, C.B. Rao, T. Jayakumar, B. Raj. A new optical technique for detection of defects in ferromagneticmaterials and components // *NDT E Int.* 2000, v. 33, p. 289-295.

12. F. Forster. Nondestructive inspection by the method of magnetic flux leakage fields // *Defektoskopia*. 1982, v. 11, p. 3-25.

13. B. Ramdane, D. Trichet, M. Belkadi, T. Saidi, J. Fo-uladgar. 3D numerical modeling of a new thermo-inductive NDT using pulse mode and pulsed phase methods // *European Physical Journal: Applied Physics, EDP Sciences*. 2010, v. 52 (2).


*Статья поступила в редакцию 16.07.2018 г.*

## ТЕРМОГРАФИЧЕСКАЯ ДЕФЕКТОСКОПИЯ МАТЕРИАЛОВ В ЯДЕРНОЙ ЭНЕРГЕТИКЕ НА ОСНОВЕ АНАЛИЗА НОРМАЛИЗОВАННОГО КОЭФФИЦИЕНТА ДИНАМИКИ ТЕРМОПРОЯВЛЕНИЯ ДЕФЕКТОВ ПРИ ИНДУКЦИОННОЙ АКТИВАЦИИ

***Н.И. Базалеев, В.В. Литвиненко***

Рассмотрены особенности индукционной термографии для дефектоскопии ферромагнитных материалов, используемых в ядерной энергетике. Предложена методика термографической дефектоскопии ферромагнитных материалов на основе динамического контрастного анализа термоизображений и нормированного коэффициента теплового проявления дефектов при электромагнитной активации образцов. Представлены материалы экспериментальных исследований, подтверждающие эффективность использования низкочастотных (50 Гц) индукторов в термографической дефектоскопии, возможность идентификации термопроявлений дефектов на фоне ложных термоаномалий путем мониторинга изменения термодинамической температуры в области дефектов во время индукционной активации.

# ТЕРМОГРАФІЧНА ДЕФЕКТОСКОПІЯ МАТЕРІАЛІВ В ЯДЕРНІЙ ЕНЕРГЕТИЦІ НА ОСНОВІ АНАЛІЗУ НОРМАЛІЗОВАНОГО КОЕФІЦІЄНТА ДИНАМІКИ ТЕРМОПРОЯВЛЕННЯ ДЕФЕКТІВ ПРИ ІНДУКЦІЙНІЙ АКТИВАЦІЇ

***М.І. Базалєєв, В.В. Литвиненко***

Розглянуто особливості індукційної термографії для дефектоскопії феромагнітних матеріалів, які використовуються в ядерній енергетиці. Запропоновано методику термографічної дефектоскопії феромагнітних матеріалів на основі динамічного контрастного аналізу термозображень і нормованого коефіцієнта теплового прояву дефектів при електромагнітній активації зразків. Представлено матеріали експериментальних досліджень, що підтверджують ефективність використання низькочастотних (50 Гц) індукторів у термографічній дефектоскопії, можливість ідентифікації термопроявлення дефектів на тлі помилкових термоаномалій шляхом моніторингу зміни термодинамічної температури в області дефектів під час індукційної активації.